Available online at www.sciencedirect.com
ScienceDirect
Journal of Computational Physics 220 (2006) 290–311
JOURNAL OF COMPUTATIONAL PHYSICS
www.elsevier.com/locate/jcp

Explicit small-scale velocity simulation for high-*Re* turbulent flows

K.A. Kemenov, S. Menon *

School of Aerospace Engineering, Georgia Institute of Technology, 270 Ferst Drive, Atlanta, GA 30332-0150, United States

Received 14 November 2005; received in revised form 18 April 2006; accepted 9 May 2006
Available online 30 June 2006

Abstract

A new approach, two level simulation (TLS), is developed based on the explicit reconstruction of the small-scale velocity by solving the small-scale governing equations on the domain with reduced dimension representing a collection of one-dimensional lines embedded in the three-dimensional flow domain. A coupled system of equations, that is not based on an eddy-viscosity hypothesis, is derived based on the decomposition of flow variables into the large-scale and the small-scale components without introducing the concept of filtering. Simplified treatment of the small-scale equations is proposed based on neglecting the small-scale advective and dissipative terms in the line orthogonal directions. Fully coupled simulation of the forced isotropic turbulence at $Re_\lambda \approx 65$, 114 demonstrates potential benefits and challenges of the TLS approach for high-*Re* turbulent flows using coarse grids.

Keywords: Turbulent flows; Large Eddy simulation; Subgrid-scale modeling

1. Introduction

Direct numerical simulation (DNS) of high-Reynolds (*Re*) number turbulent flows is computationally very expensive because of the resolution requirement needed to accurately represent the whole range dynamically important scales. Even with the advent of massively parallel computers, DNS is still limited to relatively low *Re* number turbulent flows [1,2]. Large eddy simulation (LES) approach, where only large, energy containing scales are simulated by the filtered Navier–Stokes equations with the effect of the rest of the scales modeled, has been at frontier of high-*Re* turbulent research for a long time. In LES, the large-scales are separated with help of filtering operation applied to the Navier–Stokes equations and the major effort is concentrated on modeling of the residual stress in terms of the large-scale (resolved) velocity (see, for example, recent reviews by Piomelli [3]; Meneveau and Katz [4]). The residual stress is usually referred as the subfilter stress (SFS), or the subgrid stress (SGS) depending on the meaning of the filtering operation. Proved to be very successfully

* Corresponding author. Tel.: +1 404 894 9126; fax: +1 404 894 2760.
E-mail addresses: kkemenov@gatech.edu (K.A. Kemenov), suresh.menon@aerospace.gatech.edu (S. Menon).

0021-9991/$ - see front matter
doi:10.1016/j.jcp.2006.05.006

for classical geometrically simple flows, LES is still waiting to live up to expectations to be a viable method to simulate high-*Re* complex industrial flows [5].

LES aims to describe the dynamics of the large-scale (filtered) fields which are usually obtained by applying a filter $G(\mathbf{x}, \Delta)$ to the actual fields to filter out the small-scales of the flow. For example, the filtered velocity $\bar{u}_i$ is defined as

$$\bar{u}_i(\mathbf{x}) = \int_{\Omega} u_i(\mathbf{y}) G(\mathbf{x}-\mathbf{y}, \Delta)\, \mathrm{d}\mathbf{y}, \quad \mathbf{x}, \mathbf{y} \in \Omega \subset \mathbf{R}^3 \tag{1}$$

Here, Δ is the filter width and Ω is flow domain. The filtering procedure, being a convolution integral operation, introduces unclosed terms in the LES equations which results in a complex task of creating a suitable model for the residual stress. In addition to unavoidable phenomenology introduced by the residual stress model parameters, the filtering also creates extra difficulties associated with non-commutation of the filtering operation with spatial differentiation if the filter width is not uniform [6,7]. This makes it problematic to derive LES equations in consistent way without invoking additional assumptions. It is also very difficult to relate the statistics of the filtered fields to the statistics of the experimental or direct numerical simulation data [8]. Besides, majority of practical LES applications do not use explicit filtering in the numerical integration of the filtered governing equation. It is tacitly assumed that the discrete grid representation of the flow variables can be viewed as implicitly 'grid filtered', i.e., $\tilde{u}_i$, where tilde denotes implicit filtering [9].

Assuming that filtering and differentiation commutes, which is true only for constant width explicit filters in infinite or periodic domains, non-commutation between filtering and product operations gives rise to the introduction of the residual stress $\tau_{ij} = \overline{u_i u_j} - \bar{u}_i \bar{u}_j$ into the LES equations. This residual stress is assumed to be computable during numerical simulations and needs to be modeled in terms of the resolved velocity, i.e., $\tau_{ij}(\bar{u}_i)$, in order to close the LES equations. However, as it was pointed out in a number of recent works [10,11], the replacement of $\overline{u_i u_j}$ by $\bar{u}_i \bar{u}_j + \tau_{ij}$ automatically leads to a mathematical inconsistency. This is because the convective product term $\bar{u}_i \bar{u}_j$ has the spectral support bigger than any other term in the filtered Navier–Stokes equations. As a result, the high wave number modes generated due to the non-linear interaction and extended beyond the smallest resolvable LES scale cannot be fully computed by the LES equations. In spectral space, the convective product term $\bar{u}_i \bar{u}_j$ is represented by the convolution of spectral velocity with itself, and therefore, has twice bigger spectral support than the filtered velocity $\bar{u}_i$ [12]. As a result, in practical computations the high wave number modes can alias back to the resolved part of the spectrum producing undesirable effects on the dynamics of the resolved turbulent scales. To alleviate this inconsistency and to retain the spectral content of the convective product term an additional explicit filtering is suggested in the form $\tau'_{ij} = \overline{u_i u_j} - \overline{\bar{u}_i \bar{u}_j}$ [10,11]. However, there are still drawbacks of the explicit filtering approach. In addition to the higher computational cost, the new representation of the residual stress τ'_{ij} is not Galilean invariant unless the imposed filter is a spectral cut-off filter [10,13]. This effectively diminishes the capabilities of the explicit filtered LES to study turbulent flows in complex geometries, when finite volume or finite difference schemes are employed.

To accommodate the implicit filtering action of the grid into continuous LES equation the formal superposition of explicit and implicit filtering is usually considered which leads to the doubly filtered Navier–Stokes equations for $\tilde{\bar{u}}_i$ and $\tilde{\bar{p}}$ [14]. Formally consistent, double filtering produces new types of stresses in the total residual stress decomposition. Indeed, the total residual stress arising from the double filtering can be written as a sum of subgrid large-scale stress (SGLS) and the grid filtered subfilter stress (GFSFS), i.e., $\tilde{\bar{\tau}}_{ij} = \tilde{\bar{\sigma}}_{ij} + \tilde{\bar{T}}_{ij}$, where $\tilde{\bar{\sigma}}_{ij} = \widetilde{\overline{u_j u_k}} - \widetilde{\bar{\bar{u}}_j \bar{\bar{u}}_k}$ and $\tilde{\bar{T}}_{ij} = \widetilde{\overline{u_j u_k}} - \widetilde{\overline{\bar{u}_j \bar{u}_k}}$ (see, for example [11]). This procedure requires triple and quadruple filtering application and sets additional challenges for viable modeling of the residual stresses. In practical application some additional assumptions, like commutation between the explicit filtering and implicit filtering ($\tilde{\bar{u}}_i = \tilde{\bar{u}}_i$), are usually needed [14].

There is yet another "non-commutative" feature of the filtering operation, which has received very little attention in the LES literature. In general, the filtering operation does not commute with differentiation unless the filter width is constant. Evidently, such filters are not well suited for LES studies of geometrically complex turbulent flows where high turbulence regions may coexist with weakly turbulent or laminar regions. Most works in this direction have been focused on two major approaches: the construction of explicit filters which can commute with differentiation, at least up to the order of accuracy of the numerical scheme, and the explicit

adding of the non-commutation terms into the filtered Navier–Stokes equation. Ghosal and Moin [15] proposed an explicit filtering scheme that results in the additional commutation terms which are of the second order with respect to the filter width. The construction of commutative non-uniform filters was further addressed by van der Ven [16] and Vasilyev et al. [13]. The later work uses mapping of the non-uniform grid in physical domain to the uniform grid in computational domain where the constant width filtering can be performed. This approach was further generalized by Marsden et al. [17] to construct commutative filters for unstructured grids. The second approach has received attention in the recent work of Geurts and Leonard [18] who proposed the general LES equations with included non-commutative terms. The authors emphasized, contrary to approaches which are based on the commutative filter construction, that the non-commutative terms do not vanish for any non-uniform filter and have to be accounted and modeled explicitly. However, the explicit adding of the non-commutation terms into the filtered Navier–Stokes system not only would complicate the LES equations but also would require additional modeling of these new terms analogous to the modeling of the residual stresses. A challenging task of modeling of the non-commutation terms has been further addressed in works of van der Bos and Geurts [19,20].

Accounting for these new unclosed terms adds extra challenges to the LES methodology when modeling of the near-wall turbulence is required. This area is especially critical for LES in order to become a viable predictive tool for high-Re number engineering flows. The key difficulties originate in the presence of quasi-streamwise and hairpin vortices that play a dominant dynamic role in the near-wall turbulence. To resolve these structures, a fine (comparable to DNS) grid resolution is required not only in wall normal direction but also in the spanwise and streamwise direction. Computational complexity of resolving the wall layer (minimal number of the resolved scales) is Reynolds number dependent, and approximately scales at least as $Re^{1.8}$ [21]. So far, most subgrid models perform poorly in the near-wall region when the grid resolution allows practically achievable computations.

Giving the facts that the filtering leads to extra assumptions in the derivation of the LES equations, as well as difficulties in their implementation at discrete level, it is therefore, not well suited framework for geometrically complex turbulent flows. The major objective of this work is to propose a computational framework which requires the least modeling efforts and allows treatment of complex geometry without adopting major assumptions or adding extra terms in the large-scale governing equations. Some earlier attempts of applying the current approach to simulate turbulent non-homogeneous flows, such as mixing layers or a channel flow, were reported in [22,23]. In the current study, we focus on the simulation of the forced isotropic turbulent field as well as the interpretation of our model based on *a priori* analysis of DNS data.

2. Two scale decomposition approaches

The current approach, called two level simulation (TLS), does not require explicit or implicit filtering, and provides more freedom to describe the contribution of the unresolved (small-scales) scales. It can be related to multiscale decomposition methods. Multiscale description of turbulent flows have been proposed recently by several authors including, among others, Hylin and McDonough [24] as the additive turbulent decomposition approach; Dubois et al. [25,26] as the dynamic multilevel method; Hughes et al. [27–29] as the variational multiscale method; Laval et al. [30–32] as the rapid distortion theory model.

In all these studies the total flow field is decomposed into the resolved (large-scale) u_i^{L} and the unresolved (small-scale) u_i^{S} components, i.e., $u_i = u_i^{\mathrm{L}} + u_i^{\mathrm{S}}$, and then the coupled system of the large-scale and small-scale governing equations is derived. Most of these multiscale methods, with the exception of the rapid distortion theory (RDT) model, adopt the weak formulation of the Navier–Stokes equations, which allows to view the large-scale field as a projection on a subspace spanned by the first elements of the adopted functional basis, and the small-scale field as a projection on the complement subspace. The common feature of these methods is the derivation of the small-scale governing equation which is needed for explicit computation of the small-scales. As the result, the large-scale equation can be treated as closed, since the residual stress is directly computable once the small-scale field is known.

The full coupled simulation of the large-scale and the small-scale governing equations is clearly computationally not viable since it will require DNS-like resolution to accurately represent the small-scale motions. Therefore, some physical reasoning is usually invoked to simplify the small-scale governing equation and

make it computationally tractable. For example, in the RDT model the scales are separated using standard LES filtering, and the small-scale equation is derived by subtraction of the filtered (large-scale) equation from the full Navier–Stokes equation. The small-scale equation can be simplified further by retaining only the non-linear products of the large-scale and the small-scale velocities, while all other product terms can be modeled using a turbulent viscosity and stochastic forcing, which leads to the linear form of the small-scale equation and resembles the RDT equation [30,31,33]. The approach was applied to study several cases of 2D turbulent flows as well as more complex case of the 3D decaying, isotropic turbulence, though in spectral representation. Simultaneous numerical treatment of the coupled large-scale and the small-scale equations led to an increase in computational time by a factor of 3 (!) over standard DNS [31]. The linear structure of the small-scale RDT equation was further exploited by implementing the Lagrangian time integration scheme to the Gabor transformed form of the small-scale equation [33]. Such procedure resulted in substantial saving in computational time (up to a factor of 100) for 2D turbulent simulation compared DNS. However, in spite of the simplified linear structure of the small-scale RDT equation, it still remains to be seen if the model would be applicable to treat non-homogeneous turbulent flows in complex geometries.

Another class of multiscale numerical strategies referred as the dynamic multilevel methods (DML) originates from the dynamical systems theory and the utilizes the mathematical concept of approximate inertial manifold (AIM) that can be introduced to approximate the attractor of Navier–Stokes equations. Simplification of the small-scale equation based on physical grounds, and obtained by neglecting the non-stationary term, the mixed large-scale/small-scale term and the mutual small-scale product term, leads to a relation for the AIM providing the closure for the large-scale dynamic equations [34,35]. The DML approach has been developed and applied to simulation of 2D and 3D turbulent flows by Dubois et al. [25,26], and resulted in the reduction of computational time up to a factor of 3 compared to DNS. However, most DML applications have been implemented in spectral space for homogeneous isotropic flows in periodic domains. Spectral extension of the DML to treat non-homogeneous direction in turbulent channel flow has been reported by Bouchon and Jauberteau [36]. Based on results of this work the authors suggest that the DML needs to be replaced by the multi-domain decomposition technique to separate scales in order to treat flow in complex geometries.

Recognizing high computational cost of the explicit simulation of the small-scale equation, a different approach was adopted by Hughes and co-authors [27] in developing the variational multiscale method (VMS). Instead of resolving all dynamically relevant small-scale motions, the small-scale equation is solved on a relatively coarse grid, while the ''unresolved'' part of the small-scale residual stress is modeled by using the Smagorinsky eddy-viscosity model. To separate the scales, the large-scale equation is treated on an even coarser grid, for example twice coarser grid. Thus, in the VMS approach all modeling is confined to the small-scales equations only, while the large-scale equations are closed [27]. However, as it was pointed out in [37], this is only partially true. Clearly, since the small-scales are represented by resolved modes, the unresolved portion of the small-scales still affect the large-scales, and therefore corresponding terms requires modeling rather than being neglected. The spectral VMS method with the Smagorinsky model has been successfully applied to simulate 3D decaying isotropic turbulence [28] and low Reynolds number 2D turbulent channel flow [29].

However, an extension of the VMS method for finite volume or finite difference codes implemented in physical, rather than spectral space, is a very non-trivial task. Being formulated in the weak sense, the VMS method requires construction of the complete hierarchical functional bases in physical space to separate scales by projection, which is difficult to reconcile with the finite volume or finite difference discrete representation.

The present (TLS) approach follows the general logic of multiscale decomposition methods assuming that flow fields are split into the large-scale and the small-scale components. There are two major distinctions from others multi-scale methodologies. The TLS governing equations are formulated in the strong sense, i.e., without resorting to integral form representation over corresponding trial functional spaces, and do not use notion of filtering to separate scales. This makes the approach easily adaptable for the finite volume and finite difference methods on geometrically complex, non-uniform grids. In order to reduce computational costs the small-scale equations are solved on a ''reduced'' 3D domain, rather than the full 3D flow domain. This domain represents a collection of intersecting lines embedded in the 3D domain. As a result, the small-scale governing equations along these lines can be treated in a parallel fashion, making the TLS approach computationally feasible.

The paper is organized as follows: in Section 3, we formulate the large-scale and small-scale governing equations without invoking filtering. We show that if the large-scale field is defined as the filtered quantity,

then the large-scale equations are the same as the standard LES equations. In Section 4, we formulate the 3D small-scale equations on a family of lines. Such a representation requires modeling of the transverse velocity gradients along the lines. We present a simple model based on statistical analysis of DNS data. In Section 5, we test the TLS approach for the forced isotropic turbulence simulated at two Reynolds numbers $Re_\lambda = 65$ and 114 based on the Taylor scale. Conclusions are given in Section 6.

3. Large-scale and small-scale equations

Decomposition approach is quite common in derivation of various governing equations in fluid mechanics ranging from acoustics equations to Reynolds averaged equations for turbulent flows. Here, we consider a case of the incompressible turbulent flow with uniform density ρ which can be described by velocity and pressure fields (u_i, p) and governed by Navier–Stokes equations in 3D domain Ω.

$$\frac{\partial u_i}{\partial t} + \frac{\partial u_i u_j}{\partial x_j} = -\frac{1}{\rho}\frac{\partial p}{\partial x_i} + \nu \frac{\partial^2 u_i}{\partial x_j^2}, \quad \frac{\partial u_i}{\partial x_i} = 0 \tag{2}$$

To ease further notations, we also drop density in the pressure gradient term assuming that it is included in the pressure field. When kinematic viscosity $\nu = \mu/\rho$, characteristic length L and velocity U scales of a problem are such that the Reynolds number $Re = UL/\nu$ is sufficiently high then the flow is turbulent. The challenge here is to demonstrate a computationally feasible method that can be used to simulate high-Re flows.

In the LES approach, the grid resolution requirement can be substantially lowered by considering filtered fields $(\bar{u}_i, \bar{p})$. However, the large-scale field can also be obtained without using filters. A discrete LES approach, which based on sampling of the total velocity instead of filtering has been proposed by Knaepen et al. [38] and alleviates some difficulties of the traditional LES. Very often in practical computations or experiments, flow field is known on the coarse (large-scale) grid and can be thought of as the approximations to the sampled values of the true flow fields (u_i, p). Clearly, such an interpretation of the large-scale velocity is more consistent with probe measurement in experiments than the filtered velocity field.

In order to formulate TLS governing equations without invoking a concept of filtering, we first introduce a class of the large-scale (LS) functions $\mathscr{F}^{\mathrm{L}}$. Any LS quantity which belongs to this class is denoted by superscript L, i.e., $u_i^{\mathrm{L}} \in \mathscr{F}^{\mathrm{L}}$ represents the LS velocity. Before defining the main property of the class $\mathscr{F}^{\mathrm{L}}$, we present two examples of the LS functions which can be viewed as members of $\mathscr{F}^{\mathrm{L}}$. The first one is the filtered LES velocity defined by Eq. (1). The second example can be constructed based on the underlying LS grid G^Δ and the total velocity u_i with help of the LS operator:

$$\begin{aligned} &u_i^{\mathrm{L}}(\mathbf{x}) = \mathscr{L}^\Delta u_i(\mathbf{x}) = \mathscr{I}^\Delta \circ \mathscr{S}^\Delta[u_i(\mathbf{x})], \quad \mathscr{S}^\Delta : u_i(\mathbf{x}) \to u_i^{\mathrm{L}}(\mathbf{x}_k), \mathscr{I}^\Delta : u_i^{\mathrm{L}}(\mathbf{x}_k) \to u_i^{\mathrm{L}}(\mathbf{x}), \\ &\mathbf{x}_k \in G^\Delta \equiv \{\mathbf{x}_1, \ldots, \mathbf{x}_N\} \subset \Omega \end{aligned} \tag{3}$$

Here, $\mathscr{S}^\Delta$ is a local averaging operator, $\mathscr{I}^\Delta$ is analogous to interpolation operator and acts on discrete function $u_i^{\mathrm{L}}(\mathbf{x}_k)$ mapping it to continuous LS velocity $u_i^{\mathrm{L}}(\mathbf{x})$. The local averaging operator $\mathscr{S}^\Delta$ can be quite general and time dependent. It depends on the LS grid G^Δ and the algorithm how the discrete LS value is actually obtained. The simplest case of $\mathscr{S}^\Delta$ is the sampling operator when the LS velocity values is defined as the velocity values at the nodes of G^Δ, i.e., $u_i^{\mathrm{L}}(\mathbf{x}_k) = u_i(\mathbf{x}_k)$. In more complex cases, the local averaging over some lines (one or several) or volume can be applied. The LS quantity given by (3) is unique when the averaging operator $\mathscr{S}^\Delta$ and the operator $\mathscr{I}^\Delta$ are fixed. In terms of "degrees of freedom" this construction is similar to traditional filtering since the filtered field is also defined uniquely when two parameters are specified (the functional form of filter G and the filter width Δ). However, the construction (3) is more versatile since it can allow non-uniform grids with different local clustering, thus resolving different range of scales in various parts of the flow domain.

There are infinite number of possibilities to define $\mathscr{L}^\Delta$, and generally, its exact structure is not known. Therefore, we do not define the class $\mathscr{F}^{\mathrm{L}}$ based on operator form as given by Eq. (3) or (1). In addition, $\mathscr{F}^{\mathrm{L}}$ may contain some other LS fields which cannot be represented in operator form, whether they are obtained by convolution with a filter or by means of a composite operator $\mathscr{L}^\Delta$. Instead, we will assume that for a given LS grid G^Δ, $\mathscr{F}^{\mathrm{L}} \subset C^n(\Omega \times (0, \infty))$ and consist of fields with "approximately" bounded spectral support. That means that the spectral energy content of the second derivative of the LS field decays sufficiently

fast beyond the maximal grid resolvable mode k_Δ such that we can consider the LS field and its derivatives (first and second) to have the same support. This assumption can be motivated by the fact that differentiation in physical space is equivalent to multiplication by wave number k in a spectral space, and therefore it does not enlarge the spectral support (as oppose to product operation) but merely amplify the energy content of the smallest modes.

A class of the LS fields $\mathscr{F}^{\mathrm{L}}$ gives rise to a class of the the small-scale (SS) fields based on decomposition:

$$u_i^{\mathrm{S}} = u_i - u_i^{\mathrm{L}}, \quad p^{\mathrm{S}} = p - p^{\mathrm{L}} \tag{4}$$

In other words, for any LS field $u_i^{\mathrm{L}} \in \mathscr{F}^{\mathrm{L}}$ the difference $u_i - u_i^{\mathrm{L}} \in \mathscr{F}^{\mathrm{S}}$ is considered to be the corresponding SS field and denoted by superscript S.

In spectral space, the SS field, being a complement to the total field, dominates dynamically (relative to the LS field) for modes beyond k_Δ. There also exists a δ-region around k_Δ, which corresponds to the smallest LS eddy size, where the SS field is energetically comparable with the LS field. Schematically it can be written as

$$\begin{cases} e^{\mathrm{L}}(k) \gg e^{\mathrm{S}}(k), & k < k_\Delta - \delta/2 \\ e^{\mathrm{L}}(k) \approx e^{\mathrm{S}}(k), & k_\Delta - \delta/2 < k < k_\Delta + \delta/2 \\ e^{\mathrm{L}}(k) \ll e^{\mathrm{S}}(k), & k > k_\Delta + \delta/2 \end{cases}$$

where e^{L} and e^{S} are spectral energies of LS and SS field. This is further illustrated in Fig. 1 for the case of isotropic turbulence. The LS field is explicitly computed based on 32^3 uniform grid from a forced isotropic DNS data set given on 128^3 grid [39]. The operator $\mathscr{S}^\Delta$ is the averaging along three orthogonal lines parallel to coordinates and intersecting at the LS grid cell. The operator $\mathscr{I}^\Delta$ is chosen to be the cubic spline interpolation and extends the LS field onto the DNS grid. Note that this choice of the splitting produces the SS field such that the SS energy of the modes with $k < k_\Delta$ (LS modes) is greater then the SS energy of the modes with $k > k_\Delta$ which correspond to the SS motions. In case of non-homogeneous turbulence, when non-uniform grids are used, considerations stay the same with the exception that the LS and the SS energies are functions in 3D spectral space, i.e., $e^{\mathrm{L}}(k_1,k_2,k_3)$, $e^{\mathrm{S}}(k_1,k_2,k_3)$ and k_Δ is defined as a closed surface $k_\Delta(k_1,k_2,k_3) = 0$. It is also clear that the SS field solely depends on the LS field through decomposition Eq. (4), and in principle can be quite large and even comparable to the LS fields in magnitudes. Nevertheless, we will consistently use the notion of "small-scale" to refer to such fields.

Note that in constructing the classes $\mathscr{F}^{\mathrm{L}}$ and $\mathscr{F}^{\mathrm{S}}$ we do *not* pursue the mathematical rigor. Instead, in this paper we are concerned with developing a generic *computational* framework which does not depend on filtering to describe dynamics of the LS turbulent fields.

Decomposition similar to Eq. (4) can be also applied to a product fields obtained from u_i and p. For example, the non-linear product of velocities u_iu_j can be written as a sum of the LS and the SS components:

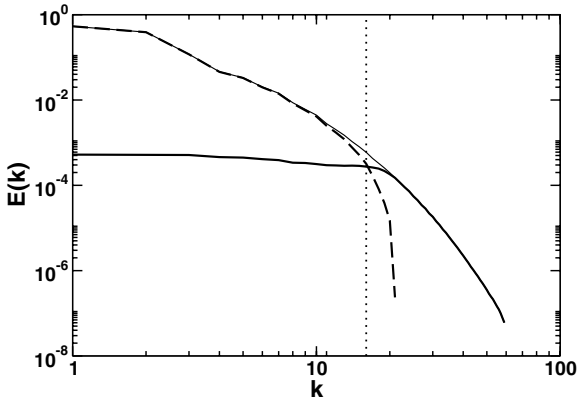

Fig. 1. SS energy (solid line), LS energy (dashed line) and total DNS energy (thin solid line) spectra for the case of isotropic turbulence. Maximal grid resolvable mode k_Δ is shown by dotted vertical line.

$$(u_i u_j)^{\mathrm{L}} + (u_i u_j)^{\mathrm{S}} = \left[\left(u_i^{\mathrm{L}} + u_i^{\mathrm{S}}\right)\left(u_j^{\mathrm{L}} + u_j^{\mathrm{S}}\right)\right]^{\mathrm{L}} + \left[\left(u_i^{\mathrm{L}} + u_i^{\mathrm{S}}\right)\left(u_j^{\mathrm{L}} + u_j^{\mathrm{S}}\right)\right]^{\mathrm{S}} \tag{5}$$

To substitute the original problem given by Navier–Stokes equation the following coupled system of the LS and the SS equations is proposed:

Proposition. *Let the LS and the SS velocity and pressure fields be such that* $u_i = u_i^{\mathrm{L}} + u_i^{\mathrm{S}}$, $p = p^{\mathrm{L}} + p^{\mathrm{S}}$, *and* u_i^{L}, $p^{\mathrm{L}} \in \mathscr{F}^{\mathrm{L}}$, u_i^{S}, $p^{\mathrm{S}} \in \mathscr{F}^{\mathrm{S}}$. *Then a coupled system of the LS and SS the equations*:

$$\frac{\partial u_i^{\mathrm{L}}}{\partial t} + \frac{\partial}{\partial x_j}\left[\left(u_i^{\mathrm{L}} + u_i^{\mathrm{S}}\right)\left(u_j^{\mathrm{L}} + u_j^{\mathrm{S}}\right)\right]^{\mathrm{L}} = -\frac{\partial p^{\mathrm{L}}}{\partial x_i} + \nu\frac{\partial^2 u_i^{\mathrm{L}}}{\partial x_j^2} \tag{6}$$

$$\frac{\partial u_i^{\mathrm{S}}}{\partial t} + \frac{\partial}{\partial x_j}\left[\left(u_i^{\mathrm{L}} + u_i^{\mathrm{S}}\right)\left(u_j^{\mathrm{L}} + u_j^{\mathrm{S}}\right)\right]^{\mathrm{S}} = -\frac{\partial p^{\mathrm{S}}}{\partial x_i} + \nu\frac{\partial^2 u_i^{\mathrm{S}}}{\partial x_j^2} \tag{7}$$

is equivalent to the original Navier–Stokes equation.

To show that Eqs. (6) and (7) can be obtained from the original Navier–Stokes equation we substitute Eq. (4) into Eq. (2). Rearranging terms produces the coupled set of the LS and the SS equations:

$$\frac{\partial u_i^{\mathrm{L}}}{\partial t} + \frac{\partial}{\partial x_j}\left(u_i^{\mathrm{L}} + u_i^{\mathrm{S}}\right)\left(u_j^{\mathrm{L}} + u_j^{\mathrm{S}}\right) = -\frac{\partial p^{\mathrm{L}}}{\partial x_i} + \nu\frac{\partial^2 u_i^{\mathrm{L}}}{\partial x_j^2} + F_i^{\mathrm{S}}\left(u_i^{\mathrm{S}}, p^{\mathrm{S}}\right) \tag{8}$$

$$\frac{\partial u_i^{\mathrm{S}}}{\partial t} + \frac{\partial}{\partial x_j}\left(u_i^{\mathrm{L}} + u_i^{\mathrm{S}}\right)\left(u_j^{\mathrm{L}} + u_j^{\mathrm{S}}\right) = -\frac{\partial p^{\mathrm{S}}}{\partial x_i} + \nu\frac{\partial^2 u_i^{\mathrm{S}}}{\partial x_j^2} + F_i^{\mathrm{L}}\left(u_i^{\mathrm{L}}, p^{\mathrm{L}}\right) \tag{9}$$

where the forcing terms on the right hand side are given as

$$F_i^{\mathrm{L}}\left(u_i^{\mathrm{L}}, p^{\mathrm{L}}\right) = -\frac{\partial u_i^{\mathrm{L}}}{\partial t} - \frac{\partial p^{\mathrm{L}}}{\partial x_i} + \nu\frac{\partial^2 u_i^{\mathrm{L}}}{\partial x_j^2} \tag{10}$$

$$F_i^{\mathrm{S}}(u_i^{\mathrm{S}}, p^{\mathrm{S}}) = -\frac{\partial u_i^{\mathrm{S}}}{\partial t} - \frac{\partial p^{\mathrm{S}}}{\partial x_i} + \nu\frac{\partial^2 u_i^{\mathrm{S}}}{\partial x_j^2} \tag{11}$$

The LS and the SS velocities affect each other through F_i^{S}, F_i^{L}, which explicitly depend only on the corresponding LS or SS fields, and the non-linear product term. It is seen that both Eqs. (8) and (9) represent the same Navier–Stokes equations, only written for different velocities u_i^{L} or u_i^{S}. In spite of the similar functional form, Eqs. (8) and (9) would describe different LS and SS evolution problems since they are subject to different boundary conditions and different forcing given by F_i^{L} and F_i^{S} respectively. Note that these intermediate LS and SS equations are dictated by decomposition $u_i = u_i^{\mathrm{L}} + u_i^{\mathrm{S}}$. This equation can be viewed as a redundant change of variables from u_i to twice bigger set of variables $\left(u_i^{\mathrm{L}}, u_i^{\mathrm{S}}\right)$. As a result, one needs to specify six governing equations to describe the problem. However, introduction of twice bigger set of variables leads to increase of dimensionality of phase space. We make use of this redundancy by exploiting properties of the LS and the SS fields to simplify Eqs. (8) and (9).

Explicitly expressing the LS and the SS parts of the non-linear term in both equations according to Eq. (5) gives another set of the LS and the SS equations:

$$\frac{\partial u_i^{\mathrm{L}}}{\partial t} + \frac{\partial}{\partial x_j}\left[\left(u_i^{\mathrm{L}} + u_i^{\mathrm{S}}\right)\left(u_j^{\mathrm{L}} + u_j^{\mathrm{S}}\right)\right]^{\mathrm{L}} = -\frac{\partial p^{\mathrm{L}}}{\partial x_i} + \nu\frac{\partial^2 u_i^{\mathrm{L}}}{\partial x_j^2} + G_i^{\mathrm{S}}\left(u_i^{\mathrm{L}}, u_i^{\mathrm{S}}, p^{\mathrm{S}}\right) \tag{12}$$

$$\frac{\partial u_i^{\mathrm{S}}}{\partial t} + \frac{\partial}{\partial x_j}\left[\left(u_i^{\mathrm{L}} + u_i^{\mathrm{S}}\right)\left(u_j^{\mathrm{L}} + u_j^{\mathrm{S}}\right)\right]^{\mathrm{S}} = -\frac{\partial p^{\mathrm{S}}}{\partial x_i} + \nu\frac{\partial^2 u_i^{\mathrm{S}}}{\partial x_j^2} + G_i^{\mathrm{L}}\left(u_i^{\mathrm{L}}, u_i^{\mathrm{S}}, p^{\mathrm{L}}\right) \tag{13}$$

Here, the LS and the SS forcing terms G_i^{S}, G_i^{L} are given by

$$G_i^{\mathrm{L}}\left(u_i^{\mathrm{L}}, u_i^{\mathrm{S}}, p^{\mathrm{L}}\right) = F_i^{\mathrm{L}}\left(u_i^{\mathrm{L}}, p^{\mathrm{L}}\right) - \frac{\partial}{\partial x_j}\left[\left(u_i^{\mathrm{L}} + u_i^{\mathrm{S}}\right)\left(u_j^{\mathrm{L}} + u_j^{\mathrm{S}}\right)\right]^{\mathrm{L}} \tag{14}$$

$$G_i^{\mathrm{S}}\left(u_i^{\mathrm{L}}, u_i^{\mathrm{S}}, p^{\mathrm{S}}\right) = F_i^{\mathrm{S}}\left(u_i^{\mathrm{S}}, p^{\mathrm{S}}\right) - \frac{\partial}{\partial x_j}\left[\left(u_i^{\mathrm{L}} + u_i^{\mathrm{S}}\right)\left(u_j^{\mathrm{L}} + u_j^{\mathrm{S}}\right)\right]^{\mathrm{S}} \tag{15}$$

Both Eqs. (12) and (13) are still equivalent to the original Navier–Stokes equation and can be re-written in a compact form:

$$G_i^{\mathrm{L}}\left(u_i^{\mathrm{L}}, u_i^{\mathrm{S}}, p^{\mathrm{L}}\right) + G_i^{\mathrm{S}}\left(u_i^{\mathrm{L}}, u_i^{\mathrm{S}}, p^{\mathrm{S}}\right) = 0 \tag{16}$$

It is seen that, under our assumption, G_i^{L} and G_i^{S} represent the LS and the SS fields, since all terms in their definitions belong to $\mathscr{F}^{\mathrm{L}}$ or $\mathscr{F}^{\mathrm{S}}$ class, respectively. In particularly, Eq. (16) holds if both the LS and the SS parts are equal to zero simultaneously:

$$G_i^{\mathrm{L}}\left(u_i^{\mathrm{L}}, u_i^{\mathrm{S}}, p^{\mathrm{L}}\right) = 0, \quad G_i^{\mathrm{S}}\left(u_i^{\mathrm{L}}, u_i^{\mathrm{S}}, p^{\mathrm{S}}\right) = 0 \tag{17}$$

To present some supportive arguments that solution given by Eq. (17) is a good candidate to be a unique solution of Eq. (16) we use a proof by contradiction. We assume that Eq. (17) is not true, i.e., $G_i^{\mathrm{L}} \neq 0$. As a result, G_i^{L}, being the LS field, has substantial non-zero energy in LS modes. Without loss of generality one can assume that most energy is concentrated at some wave number $k_{\mathrm{L}} < k_{\Delta}$ which is well into the LS spectral content, as shown schematically in Fig. 2(a). From Eq. (13) it is seen that G_i^{L} is the forcing term for the SS velocity field u_i^{S}. Therefore, the solution of the SS equation subject to the LS forcing would cause the SS energy e^{S} not to be small in comparison with the LS energy e^{L} for the LS mode spectral content ($k < k_{\Delta}$), which contradicts to the definition of the SS velocity field since $u_i^{\mathrm{S}} \notin \mathscr{F}^{\mathrm{S}}$.

Thus the LS spectral content of G_i^{L} should be negligible or zero in the neighborhood of k_{L}. If one moves k_{L} towards the cut-off wave number k_{Δ}, then it is clear that the same reasoning can be applied up to the δ-neighborhood of k_{Δ}. As a result, G_i^{L} should be zero function, or a function which is negligible everywhere, except the δ-neighborhood of k_{Δ}, as shown in Fig. 2(b). From Eq. (16), it is seen that G_i^{S} should be also zero function, or the same function as G_i^{L} (with an opposite sign) and with the same spectral content negligible everywhere and peaking at k_{Δ}. This can be written schematically as

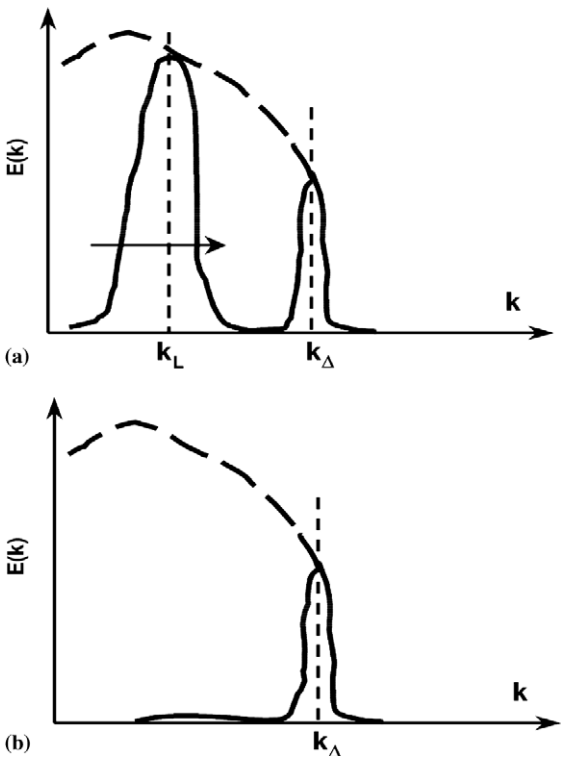

Fig. 2. (a) Sketch of the assumed spectral energy of G_i^{L} forcing term; (b) sketch of a possible spectral energy of G_i^{L} which would satisfy $G_i^{\mathrm{L}} + G_i^{\mathrm{S}} = 0$. Note that G_i^{L} does not represent neither the LS field nor the SS field. Typical spectral energy of the LS field is shown by dashed line. Maximal grid resolvable mode k_{Δ} and LS mode k_{L} are shown by dashed vertical lines.

$$\begin{cases} e^{\mathrm{L}}(k) \approx e^{\mathrm{S}}(k) \approx \varepsilon, & k < k_{\Delta} - \delta/2 \\ e^{\mathrm{L}}(k) \approx e^{\mathrm{S}}(k) \approx e^{\Delta}, & k_{\Delta} - \delta/2 < k < k_{\Delta} + \delta/2 \\ e^{\mathrm{L}}(k) \approx e^{\mathrm{S}}(k) \approx \varepsilon, & k > k_{\Delta} + \delta/2 \end{cases}$$

with $\varepsilon \ll e^{\Delta}$.

It is now seen that being this non-zero function, G_i^{L} and G_i^{S} both lose their LS and SS properties, and do not belong to $\mathscr{F}^{\mathrm{L}}$ and $\mathscr{F}^{\mathrm{S}}$ classes anymore. Clearly, G_i^{L} and G_i^{S} do not have substantial LS or SS energy contents over the corresponding range of scales, thus $G_i^{\mathrm{L}} \notin \mathscr{F}^{\mathrm{L}}$ and $G_i^{\mathrm{S}} \notin \mathscr{F}^{\mathrm{S}}$. In fact, they become indistinguishable, and the decomposition loses its meaning. Therefore, Eq. (17) must be hold, since zero function is the only element which belongs to both $\mathscr{F}^{\mathrm{L}}$ and $\mathscr{F}^{\mathrm{S}}$ classes simultaneously. Substituting Eq. (17) into Eq. (12) and (13) gives the LS equation (6) and the SS equation (7). Note that the spectral overlap between u_i^{L} and u_i^{S} does not affect these arguments since they are applied to the forcing terms G_i^{L} and G_i^{S} only.

A proof in the opposite direction follows immediately, if one adds Eq. (6) and (7). Then, it is seen that the sum of the LS and the SS solutions $u_i^{\mathrm{L}} + u_i^{\mathrm{S}}$, $p^{\mathrm{S}} + p^{\mathrm{L}}$ satisfies the original Navier–Stokes equations.

The forcing terms F_i^{S}, F_i^{L} can also be written in alternative form. Eqs. (14) and (15) give

$$F_i^{\mathrm{L}} = \frac{\partial}{\partial x_j}\left[\left(u_i^{\mathrm{L}} + u_i^{\mathrm{S}}\right)\left(u_j^{\mathrm{L}} + u_j^{\mathrm{S}}\right)\right]^{\mathrm{L}}, \quad F_i^{\mathrm{S}} = \frac{\partial}{\partial x_j}\left[\left(u_i^{\mathrm{L}} + u_i^{\mathrm{S}}\right)\left(u_j^{\mathrm{L}} + u_j^{\mathrm{S}}\right)\right]^{\mathrm{S}} \tag{18}$$

As a result, the non-linear convective term in the SS equation represents the SS part of the total convective term and can be further rewritten in a more convenient form. Substituting Eq. (18) into Eq. (7) gives the equivalent form of the SS equation:

$$\frac{\partial u_i^{\mathrm{S}}}{\partial t} + \frac{\partial}{\partial x_j}\left(u_i^{\mathrm{L}} + u_i^{\mathrm{S}}\right)\left(u_j^{\mathrm{L}} + u_j^{\mathrm{S}}\right) = -\frac{\partial p^{\mathrm{S}}}{\partial x_i} + \nu\frac{\partial^2 u_i^{\mathrm{S}}}{\partial x_j^2} + F_i^{\mathrm{L}} \tag{19}$$

Remark 1. The LS equation (6) is, in fact, the standard LES equation. Rewriting the LS equation using LES notation, i.e., $u_i^{\mathrm{L}} \to \bar{u}_i$, $u_i^{\mathrm{S}} \to u_i'$, $p^{\mathrm{L}} \to \bar{p}$ gives

$$\frac{\partial \bar{u}_i}{\partial t} + \frac{\partial}{\partial x_j}\overline{\bar{u}_i\bar{u}_j} = -\frac{\partial \bar{p}}{\partial x_i} + \nu\frac{\partial^2 \bar{u}_i}{\partial x_j^2} - \frac{\partial}{\partial x_j}\left(\overline{u_i u_j} - \overline{\bar{u}_i\bar{u}_j}\right) \tag{20}$$

where the last term represents the derivative of the residual stress $\tau_{ij} = \overline{u_i u_j} - \overline{\bar{u}_i\bar{u}_j} = \overline{u_i' u_j'} + \overline{\bar{u}_i u_j'} + \overline{u_i'\bar{u}_j}$ In LES, Eq. (20) is usually derived by filtering of the original Navier–Stokes equations and assuming commutativity between filtering and differentiation. Similarly Eq. (6) can be formally obtained by applying $\mathscr{L}^{\Delta}$ to the original Navier–Stokes equation, and further assuming its commutativity with differentiation. However, the formal application of $\mathscr{L}^{\Delta}$ to derive the LS equation is questionable on at least two accounts. First, it implicitly assumes that the LS solution should be sought only in particular form, as defined by specific structure of $\mathscr{L}^{\Delta}$, which is not known in general. This might effectively narrow the LS class $\mathscr{F}^{\mathrm{L}}$. Second, the intermediate presence of the discrete averaging operator $\mathscr{S}^{\Delta}$ might potentially destroy the well-posedness of the LS problem (which should be desired criterion for mathematically consistent LS models [40]). For these reasons in the present formulation we do not derive the LS equations based on formal application of $\mathscr{L}^{\Delta}$, or filtering.

Remark 2. Similar qualitative reasoning which was used to justify Eq. (17) can be also applied to the continuity constraint, which leads to the LS and SS equations, $\nabla_i u_i^{\mathrm{L}} = r$ and $\nabla_i u_i^{\mathrm{S}} = -r$. Here, a function $r(\mathbf{x})$ is zero, or has a negligible energy content everywhere except a neighborhood of k_{Δ}. To satisfy a requirement of being the LS and the SS field simultaneously, one has to choose $r(\mathbf{x}) = 0$ which results in the LS and the SS continuity equations:

$$\frac{\partial u_i^{\mathrm{L}}}{\partial x_i} = 0, \quad \frac{\partial u_i^{\mathrm{S}}}{\partial x_i} = 0 \tag{21}$$

Physically, such an interpretation of $r(\mathbf{x})$ has also clear meaning by specifying incompressible the LS and the SS velocity fields, as opposed to a case where $r(\mathbf{x}) \neq 0$. By considering different k_Δ, it is seen that in latter case $r(\mathbf{x})$ should depend on k_Δ which leads to unclear physical constraints for the LS and the SS velocities.

In summary, the coupled system of Eqs. (6) and (19) along with the constraint (21) supplied by appropriate initial and boundary conditions completely defines evolution of the LS and the SS fields in TLS approach.

4. Treatment of the 3D small-scale equation

Numerical simulation of the 3D SS equation is computationally challenging since it would require the resolution of the whole range of small-scales. On the other hand, the LS equation is solved on a coarse LS grid with a time step comparable to the characteristic turnover time of the smallest resolvable LS eddy. As a result, the complete knowledge of the SS field in space and time is not necessary since one only needs to know the SS fields on the LS grid at the LS time scale in order to close the LS equation.

To reduce computational expenses, while retaining two-way coupling between the LS and the SS fields, the SS equation (Eq. (19)) is solved on a collection of 1D lines embedded in domain Ω, rather than in the whole domain Ω. In general, there are no any restrictions on the position of lines in Ω and their curvature. Here, for simplicity, we consider a family of lines $\Omega_l = \{l_k^j\}$, $k = 1,2,3$, $j = 1,\ldots,N_k$, which consists of $\sum_k N_k$ lines that are parallel to the corresponding LS coordinates $\{x_k\}$ and intersect each other at the LS grid nodes as shown in Fig. 3, and introduce the SS fields defined on these lines as

$$u_i^{\mathrm{S}}(\mathbf{x},t) \to u_{i,l_k}^{\mathrm{S}}(l_k,t), \quad \mathbf{x} \in l_k \subset \Omega \tag{22}$$

The SS field u_{i,l_k}^{S} is viewed as a snapshot of the SS turbulent velocity along line l_k.

In TLS we resolve the SS field in the domain Ω_l only, while the LS field is simulated in Ω. Assuming that one needs N_{S}^3 points to resolve the smallest dynamically important scales for DNS, and N_{L}^3 points to resolve the large-scale dynamics, as in LES, results in the TLS resolution requirement of $N_{\mathrm{L}}^3 + 3N_{\mathrm{L}}^2 N_{\mathrm{S}}$ points to represent both the LS and the SS fields. Thus, the TLS approach would fall in a category between DNS and LES. However, it is often the case for LES that N_{L}^3 has to be quite high ($N_{\mathrm{L}} \to N_{\mathrm{S}}$) in highly turbulent regions, for example near walls, to accurately predict the LS dynamics because of the inherent limitations of the SGS models [41]. In TLS, since the LS and the SS are explicitly coupled, the less severe resolution requirements are

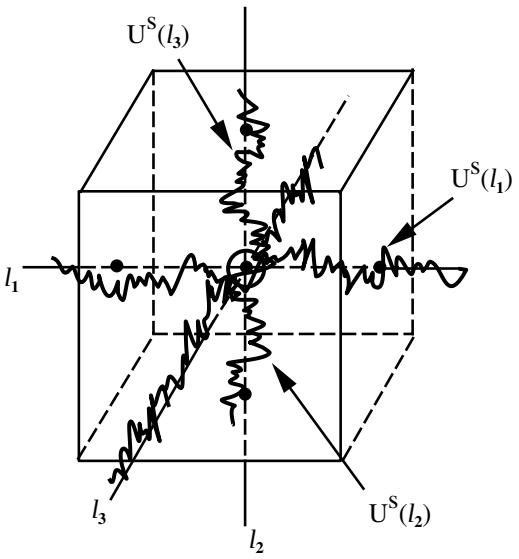

Fig. 3. The SS 1D line arrangement within a 3D LS grid cell in the TLS model. One component of the SS velocity is shown on each line schematically.

expected. In addition, simulation of the SS fields on the 1D lines, which requires $3N_{\mathrm{L}}^2 N_{\mathrm{S}}$ point resolution, can be done in parallel, thereby, reducing computational cost substantially.

Treating the SS fields on the reduced domain Ω_l is computationally more efficient, but there is a price to pay. When written on a line, say $l_1 = \{x_1, x_2 = C_2, x_3 = C_3\}$, where C_2, C_3 are constants, the SS equation (19) is not closed and requires knowledge of the first derivatives of the SS velocity and pressure, and the second derivatives of SS velocity in the directions l_2, l_3 (which are orthogonal to the line l_1). Thus, all derivatives of the SS fields in transversal directions to a given line have to be modeled, although, all derivatives along the line can be computed as a part of solution. The second difficulty arise from the fact that at the LS grid nodes, where the lines l_k intersect, the SS field becomes overdetermined since its values can be found from all three intersecting lines, and these values are not necessarily the same. Explicit requirement to have unique values of the SS fields at the LS grid points would lead to coupling of SS fields on different lines at those points, and therefore, is not viable computationally. Instead, we decouple the SS field computations on lines, which means that the SS fields do not interact each other if they belong to different lines. At the same time all realizations are still used to obtain the SS fields on the LS grid. Thus, the value of the SS fields at the node $\{\mathbf{x}_n\}$ of the LS grid cell V_n is defined as an average over all three lines belonging to V_n and intersecting at $\{\mathbf{x}_n\}$, which is essentially an operational definition of $\mathscr{S}^{\Delta}$ operator (Eq. (3)). For example,

$$\begin{aligned}\left[u_i^{\mathrm{S}}\right]^{\mathrm{L}}(\mathbf{x}_n,t) &\leftarrow \left[u_{i,l_k}^{\mathrm{S}}(l_k,t)\right]_{l_k}, \quad \left[u_i^{\mathrm{S}}u_j^{\mathrm{L}}\right]^{\mathrm{L}}(\mathbf{x}_n,t) \leftarrow \left[u_{i,l_k}^{\mathrm{S}}u_{j,l_k}^{\mathrm{L}}(l_k,t)\right]_{l_k}\left[u_i^{\mathrm{S}}u_j^{\mathrm{S}}\right]^{\mathrm{L}}(\mathbf{x}_n,t)\\ &\leftarrow \left[u_{i,l_k}^{\mathrm{S}}u_{j,l_k}^{\mathrm{S}}(l_k,t)\right]_{l_k}, \quad \{\mathbf{x}_n\} = \bigcap_{k=1}^{3} l_k, \quad l_k \cap V_n \neq \emptyset\end{aligned} \tag{23}$$

where the local average over intersecting orthogonal lines l_k in the cell V_n is denoted as $[\ ]_{l_k}$. Note that in order to close the LS equations we need know the LS values of the mutual product of the SS velocities $u_i^{\mathrm{S}}u_j^{\mathrm{S}}$ and the mixed products $u_i^{\mathrm{S}}u_j^{\mathrm{L}}$, $u_i^{\mathrm{L}}u_j^{\mathrm{S}}$ rather than the SS velocity itself. Explicit computation of these SGS terms requires knowledge of the SS velocity on each line.

Here, we propose the following model assumptions (justified, in part, by *a priori* analysis of DNS data and by *a posteriori* study of high-*Re* forced isotropic turbulence) which provide the necessary simplification for the SS equation and enable us to estimate the unknown SS velocity on lines l_k. These assumptions allow to express the unknown (transverse) SS derivatives in terms of the known (longitudinal) SS derivatives, and are following:

(i) For each SS velocity component u_i^{S}, the SS second derivative along the line l_k is equal to the averaged sum of the SS second derivatives along all three orthogonal directions:

$$\frac{\partial^2 u_i^{\mathrm{S}}}{\partial x_k^2} = \frac{1}{3}\sum_{j=1}^{3}\frac{\partial^2 u_i^{\mathrm{S}}}{\partial x_j^2}, \quad i,k = 1,2,3 \tag{24}$$

(ii) Changes of the SS part of the convective derivatives of the SS velocity components are neglected in directions transverse ($j \neq k$) to the line l_k:

$$\frac{\partial}{\partial x_j}\left[\left(u_j^{\mathrm{S}} + u_j^{\mathrm{L}}\right)\left(u_i^{\mathrm{S}} + u_i^{\mathrm{L}}\right)\right]^{\mathrm{S}} = \frac{\partial}{\partial x_j}\left[\left(u_j^{\mathrm{S}}(l_k) + u_j^{\mathrm{L}}\right)\left(u_i^{\mathrm{S}}(l_k) + u_i^{\mathrm{L}}\right)\right]^{\mathrm{S}} \tag{25}$$

These assumptions lead to the simplified form of the SS equation on each line l_k:

$$\frac{\partial u_i^{\mathrm{S}}}{\partial t} + \frac{\partial}{\partial x_j}\left[\left(u_j^{\mathrm{S}}(l_k) + u_j^{\mathrm{L}}\right)\left(u_i^{\mathrm{S}}(l_k) + u_i^{\mathrm{L}}\right)\right] = 3\nu\frac{\partial^2 u_i^{\mathrm{S}}}{\partial x_k^2} + F_i^{\mathrm{L}}\left(u_j^{\mathrm{S}}(l_k), u_j^{\mathrm{L}}\right), \tag{26}$$

where

$$F_i^{\mathrm{L}}\left(u_j^{\mathrm{S}}(l_k), u_j^{\mathrm{L}}\right) = \frac{\partial}{\partial x_j}\left[\left(u_j^{\mathrm{S}}(l_k) + u_j^{\mathrm{L}}\right)\left(u_i^{\mathrm{S}}(l_k) + u_i^{\mathrm{L}}\right)\right]^{\mathrm{L}}$$

Note, here k is a free index and refers to a line l_k which is parallel to the corresponding coordinate x_k. Thus, for different lines Eq. (26) produces different equations for the same SS velocity component. For example, for lines l_1, l_2 and u_1^S we have:

$$\frac{\partial u_1^S}{\partial t} + \frac{\partial}{\partial x_j}\left(u_j^L + u_j^S(l_1)\right)\left(u_1^L + u_1^S(l_1)\right) = 3\nu\frac{\partial^2 u_1^S}{\partial x_1^2} + F_1^L\left(u_j^S(l_1), u_j^L\right) \tag{27}$$

$$\frac{\partial u_1^S}{\partial t} + \frac{\partial}{\partial x_j}\left(u_j^L + u_j^S(l_2)\right)\left(u_1^L + u_1^S(l_2)\right) = 3\nu\frac{\partial^2 u_1^S}{\partial x_2^2} + F_1^L\left(u_j^S(l_2), u_j^L\right) \tag{28}$$

To solve Eq. (26), boundary conditions for the SS velocity field have to be specified. In our case of the forced isotropic turbulence, the periodic boundary conditions are assumed for all lines. For more complex, non-homogeneous flows, the SS boundary conditions are specified depending on the line position, and have to be consistent with the definition of the SS based on decomposition (Eq. (4)).

In Eq. (26) the SS pressure gradient $\partial p^S/\partial x_i$ is explicitly excluded. In other words, we relax the divergence-free requirement for the SS velocity along the line l_k, i.e. , $\partial u_j^S/\partial x_j \neq 0$. In principle, the SS pressure can be included in Eq. (26) by specifying the LS pressure, and an additional equation for the SS pressure. For example, taking the divergence of Eq. (8) and using Eq. (21) we have:

$$\frac{\partial^2 p^S}{\partial x_i^2} = -\frac{\partial^2 p^L}{\partial x_i^2} - \frac{\partial\left(u_i^L + u_i^S\right)}{\partial x_j}\frac{\partial(u_j^L + u_j^S)}{\partial x_i} \tag{29}$$

In our case, the non-enforcement of the SS continuity is an artifact of the incompressible fluid model and the adopted numerical approach. The continuity equation is used for the LS velocity only, and implemented according to the standard fractional step (projection) method by computing intermediate non-divergence free LS velocity field. If the current approach is adopted for a compressible flow then the continuity requirement will appear naturally as a separate governing equation for the SS density.

There is a noticeable lack of comprehensive analysis of the SS velocity derivatives in LES literature. Most studies are concerned with modeling of the SGS stress which represents the LS quantity and do not require explicit knowledge of the SS fields or their derivatives. Here, to address the model assumptions (i) and (ii) from a physical point of view, we conduct *a priori* statistical analysis of a high-Re forced isotropic turbulence DNS data set [39]. The turbulent velocity field corresponds to a Taylor scale Reynolds number $Re_\lambda \approx 140$ and is given on a box of 256^3 grid points. The LS field is computed based on the uniform 32^3 LS grid using cubic spline interpolation, and then subtracted from the total velocity to obtain the SS velocity.

4.1. Assumption (i)

The model assumption (i), Eq. (24), corresponds to the case when the difference between the SS second derivative in particular direction l_k and the averaged sum of the SS second derivatives in all three directions is equal to zero, i.e., $S_{ik} = 0$ where $S_{ik} = (\sum_{j=1}^{3}\partial^2 u_i^S/\partial x_j^2)/3 - \partial^2 u_i^S/\partial x_k^2$. This is supported by Fig. 4(a) and (b) where all nine $(i,k = 1,2,3)$ normalized probability density functions (PDF) $f(S_{ik})$ are shown. It is interesting to note that they all fit the Tsallis distribution quite well for wide range of probabilities. The Tsallis distribution was used in the context of turbulence by Beck [42]. It has a form $P_T(\xi) = 1/(Z_q[1 + (1/2)\beta(q-1)\xi^2]^{1/(q-1)})$ where Z_q is a normalization constant and $\beta = 2/(5-3q)$ is chosen to give a unit variance. It also reduces to a Gaussian distribution as $q \to 1$. These figures show that the most probable state for the derivative differences S_{ik} is zero, or the second derivatives in orthogonal direction are equal each other with a very high probability.

These PDFs exhibit the most probable state at the origin ($S_{ik} = 0$). In other words dissipative influence of low probable and rare events characterized by $S_{ik} \neq 0$ is excluded from consideration by adoption of Eq. (24). However, this approximation can still adequately account for dissipative influence of high gradient events which dominate turbulent flow regions. Conceptually, one can divide events where $S_{ik} = 0$ in two qualitatively different groups. The first group represents a case when the SS second derivatives are small, so the differences S_{ik} are small too. Physically, points with this property would correspond to weakly turbulent flow regions which are adequately represented by the resolved LS. The second group corresponds to a case when the SS

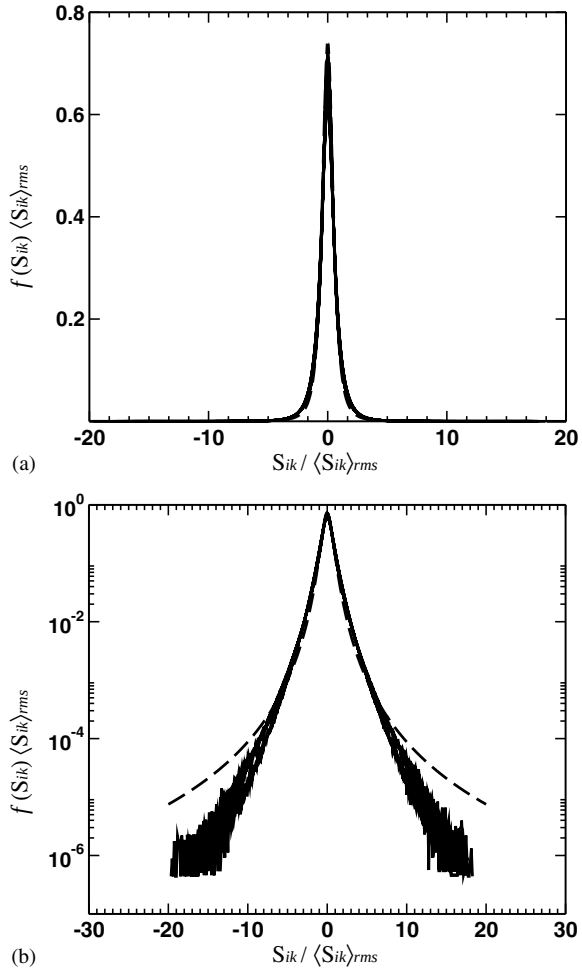

Fig. 4. PDFs of the normalized differences of the second SS derivatives, $S_{ik} = (\sum_{j=1}^{3} \partial^2 u_i^S/\partial x_j^2)/3 - \partial^2 u_i^S/\partial x_k^2$ compared with the Tsallis distribution (dashed line): (a) in linear scale, (b) in logarithmic scale. Note that all nine PDFs are shown here.

second derivatives are not small and approximately equal each other. These flow regions are characterized by intense turbulence, high dissipation and pronounced effect of the SS on the LS dynamics.

This can be clarified further by considering the joint PDFs of $(\sum_{j=1}^{3} \partial^2 u_i^S/\partial x_j^2)/3$ and $\partial^2 u_i^S/\partial x_k^2$ which are shown in Fig. 5(a) and (b). It is seen that at the origin the joint PDF exhibits a characteristic spike. Contour lines for high probabilities are approximately oval in shape and elongated along a bisector of I and III quadrants. For lower values of probability the contour lines resemble parallelograms with smoothed corners. We also note that events where the second derivative $\partial^2 u_i^S/\partial x_k^2$ is large in magnitude and has the same sign as the averaged sum $(\sum_{j=1}^{3} \partial^2 u_i^S/\partial x_j^2)/3$ are more probable and provide major contribution to the tail of the joint PDF. Therefore, with high probability, we may expect that in intense turbulent regions if the second derivative of the SS velocity component is large in magnitude in one particular direction it should be large and of the same sign in other two orthogonal directions.

The bisector of I and III quadrants corresponds to the model assumption (i), $S_{ik} = 0$. It is seen that events from the first group occur in the neighborhood of the origin and happen with the highest probability. As we move along the diagonal from the origin the magnitude of the SS second derivative increases, probability decreases, suggesting the presence of highly turbulent regions where the LS resolution becomes inadequate. Note that the model assumption $S_{ik} = 0$ corresponds to the delta function PDF at the origin, see Fig. 4(a) and (b). As a result, all events which correspond to $S_{ik} \neq 0$ are formally excluded from the consideration.

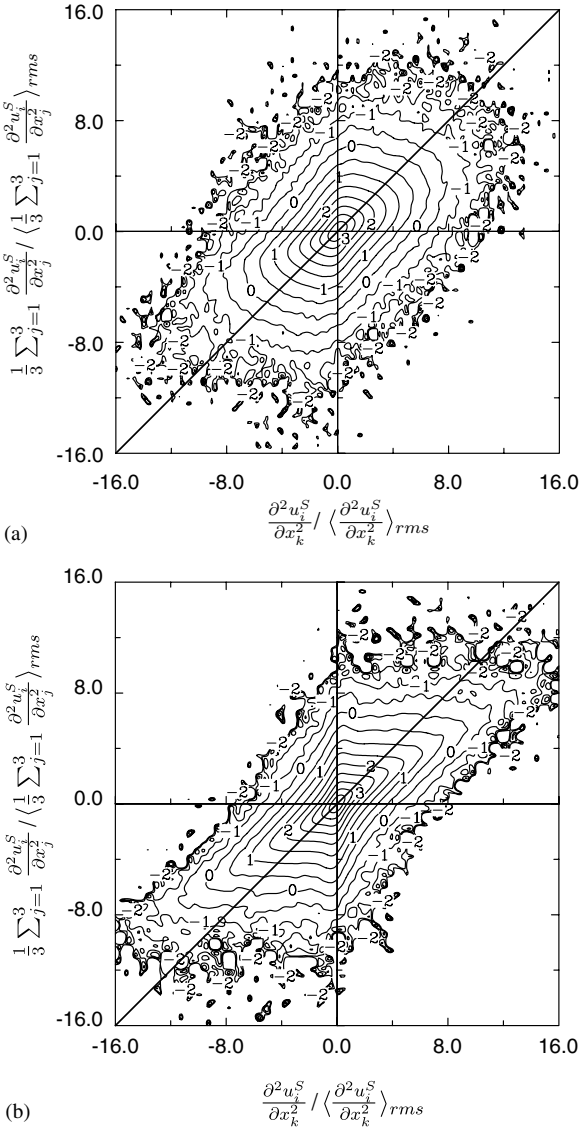

Fig. 5. Contour plots of the logarithm of the joint PDF of the normalized SS second derivative along the line l_k and the averaged sum of the SS second derivatives: (a) longitudinal velocity component $i = k$, (b) transverse velocity component $i \neq k$.

However, as suggested by Figs. 5(a) and (b) the model is not "blind" to the presence of intense SS turbulent structures. Large values of SS second derivatives are still allowed on the diagonal $S_{ik} = 0$.

For the further qualitative interpretation of the model assumption $S_{ik} = 0$ we consider the joint PDF as shown in Fig. 6 for the case of the SS longitudinal derivative ($i = k$). Assume that the SS second derivative is sufficiently large and correspond to the point A suggesting the presence of the high turbulence region. A vertical plane through A and orthogonal to the x-axis defines a conditional PDF $f((\sum_{j=1}^{3}\partial^2 u_i^S/\partial x_j^2)/3|\partial^2 u_i^S/\partial x_k^2 = a)$. It is seen that this conditional PDF is positively skewed giving the the most probable value of the averaged sum $(\sum_{j=1}^{3}\partial^2 u_i^S/\partial x_j^2)/3$ around point B. On the other hand, the line defined by the model assumption $S_{ik} = 0$ intersects with the conditional plane at point C. Due to the shape of the joint PDF, point C will always stay higher (or lower) than the maximum point B if $\partial^2 u_i^S/\partial x_k^2$ is positive (or negative) and sufficiently large in magnitude. Thus, the model assumption $S_{ik} = 0$ makes the larger value of the sum of the SS second derivative more probable which can be viewed as if the value of local viscosity is higher, which means that the SS vortical structures are more dissipative.

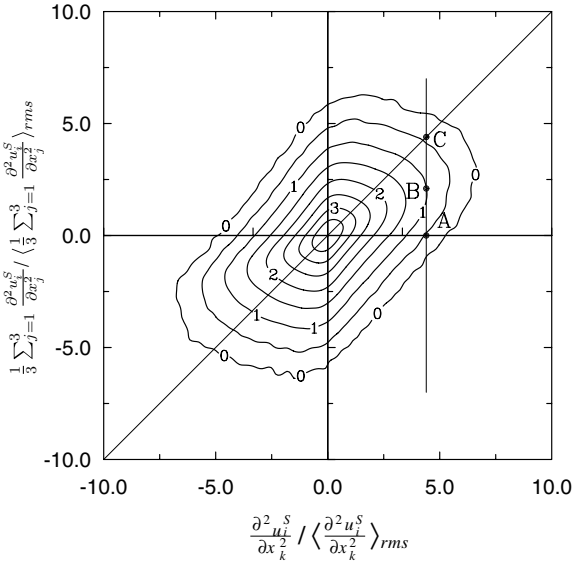

Fig. 6. Point (B) – the most probable value of the averaged sum of the SS second derivatives given the value of the SS second derivative along the line l_k at point (A), point (C) corresponds to the model assumption.

4.2. Assumption (ii)

The model assumption (ii) (Eq. (25)) allows to represent the SS line equations in the closed form. Physically it means that the SS effects that are caused by advection of the SS velocity, in the line orthogonal directions, are small in comparison the SS effects due to the advection of the LS field. To show this it is convenient to rewrite assumption (ii) in non-conservative form with the help of the continuity equation:

$$\begin{aligned}\frac{\partial}{\partial x_j}\left[\left(u_j^{\mathrm{S}}+u_j^{\mathrm{L}}\right)\left(u_i^{\mathrm{S}}+u_i^{\mathrm{L}}\right)\right]^{\mathrm{S}} &= \frac{\partial}{\partial x_j}\left(u_j^{\mathrm{S}}+u_j^{\mathrm{L}}\right)\left(u_i^{\mathrm{S}}+u_i^{\mathrm{L}}\right)-F_i^{\mathrm{L}}\left(u_i^{\mathrm{L}},u_i^{\mathrm{S}}\right)\\ &= \left(u_k^{\mathrm{S}}(l_k)+u_k^{\mathrm{L}}\right)\frac{\partial}{\partial x_k}\left(u_i^{\mathrm{S}}(l_k)+u_i^{\mathrm{L}}\right)+\underbrace{\left(u_j^{\mathrm{S}}(l_k)+u_j^{\mathrm{L}}\right)\frac{\partial u_i^{\mathrm{L}}}{\partial x_j}}_{j\neq k}-F_i^{\mathrm{L}}\end{aligned} \tag{30}$$

Note that the SS advection term is fully accounted along line l_k since derivatives of the SS velocity are always available.

Contours plots of the joint PDFs of the total SS convective terms and the modeled SS convective terms are exhibited in Figs. 7(a)–(c). Three cases are shown, which correspond to different orientation of the velocity components and the line l_k. It is seen that the contour lines have similar oval shapes for high probabilities corresponding to the small values of the SS convective terms. As the magnitude of the SS convective terms grows and the probability sharply decreases, the contour plots start resembling rectangular which is stretched along the bisector of I and III quadrants. The shape of PDFs is also almost independent of the direction of the SS convective derivatives. SS events, when both the total and the modeled SS convective terms have the same sign are more dominant. Due to a rectangular shape of the PDFs, a similar qualitative reasoning, which has been used for the SS second derivatives, is applicable here too (see Fig. 6). Accordingly, the model assumption (ii) would correspond to a case when the SS convective derivatives consistently admit values higher in magnitude than the most probable values of the total SS convective derivatives. Qualitatively, it means that the modeled SS field is subject to higher distortion by the SS advection than the exact SS field.

The SS equation (26) allows reconstruction of the SS velocity on line l_k if the LS velocity is known. Physically, the LS velocity evolves on a slower time scale than the SS velocity and requires discretization with a bigger time step. To close the LS equation it is not necessary to resolve the fast SS dynamics at all times,

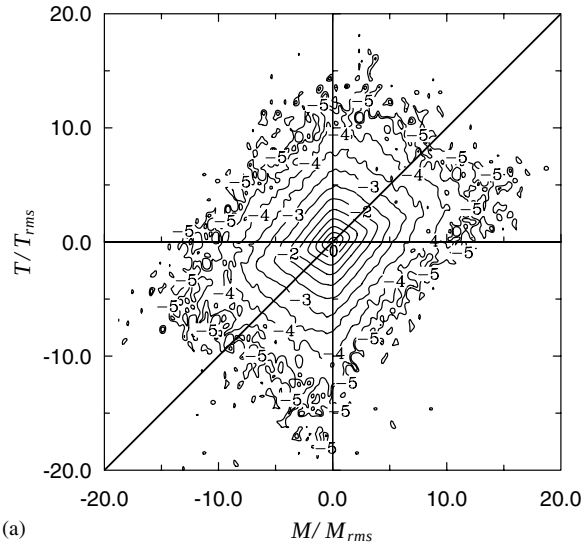

(a)

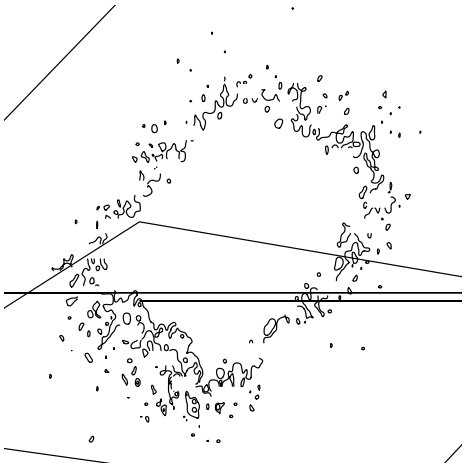

one only needs to know the SS velocity field at particular instants of the slow LS time t_m^{L}. To achieve this one can integrate Eq. (26) in small neighborhood of t_m^{L} treating the LS velocity as time independent field. In other words, for any LS time t_m^{L} and a small parameter $\epsilon \ll 1$, we introduce a local time coordinate $t^{\mathrm{S}} = \epsilon t$ according to the transformation: $t \to t_m^{\mathrm{L}} + t^{\mathrm{S}}$ such that $u^{\mathrm{L}}(l_k, t) \to u^{\mathrm{L}}(l_k, t_m^{\mathrm{L}})$ and $u^{\mathrm{S}}(l_k, t) \to u^{\mathrm{S}}(l_k, t_m^{\mathrm{L}} + t^{\mathrm{S}})$. The SS velocity evolves from zero initial state and depends only on the LS velocity and its derivatives.

Physically, evolution of the SS velocity according to Eq. (26) is interpreted as the propagation of energy disturbances down into the SS part of the turbulent spectrum due to non-linear interaction. Starting from a zero initial state, the SS velocity starts growing, continuously exciting smaller scales until the viscous dissipation region is reached. The term $\left[u_i^{\mathrm{L}} u_j^{\mathrm{L}}\right]^{\mathrm{S}}$, which is the only non-zero term at $t^{\mathrm{S}} = 0$, acts as a constant source of energy for the small-scales, triggering the forward energy cascade. We point out that even though the LS velocity is kept fixed in time t^{S}, this problem does not constitute an evolution of the SS velocity in the "frozen" LS environment. The time t^{S} corresponds to the time needed to "fill up" the SS part of the spectrum. As a

result, the SS velocity at some instant of time t^{L}_m does not depend on the SS solution at previous time t^{L}_{m-1}, i.e., it is memoryless, and is solely defined by the LS velocity and its derivatives at t^{L}_m. This is illustrated in Figs. 8 and 9. The SS velocity and the SS spectral energy are shown for three consecutive instants of time t^{S}. Due to non-linear interactions between the LS and the SS fields, energy starts cascading down to the SS part of spectrum eventually creating the SS velocity field. It is seen that at the final stage the SS energy spectrum matches the SS part of DNS spectrum quite well.

The evolution time needed to reconstruct the SS velocity field is determined by matching the LS and the SS energies at the minimal scale resolvable by the LS grid. Clearly, this time is unique for different lines and fully defined by the LS velocity, its derivatives and viscosity. Isotropic velocity field and parallel line arrangements allow us to consider an average energy along lines, which is given in Fig. 10. Here, the averaged (along l_1 lines) SS spectrum is shown with the DNS and exact SS energy spectra. It is seen that the overall comparison of the SS spectra is quite satisfactory. However, the averaged SS spectrum exhibits small deviation from the exact SS spectrum by redistributing more SS energy in favor of smaller scales, closer to dissipation range. This is probably a manifestation of the adopted assumption given by Eq. (25).

Numerical implementation of TLS is based on simulation of the LS field coupled with the SS equations which approximate the SS turbulent dynamics on lines. The line arrangement constitutes an important part of the SS model. The optimal line placement and its affect on the reconstructed SS field, due to neglecting of transverse SS advection, on its own present a non-trivial, challenging problem. In the ideal case the lines are exact streamlines of the SS velocity field. Here, we adopt a three orthogonal line arrangement where lines intersect at the center of the LS grid nodes. Given the LS and the SS grid arrangements, there are four steps involved in TLS algorithm:

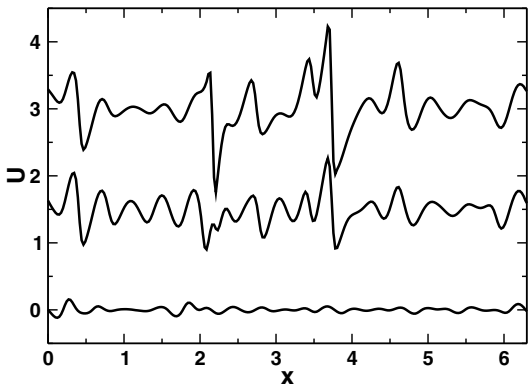

Fig. 8. Time evolution the SS velocity profile on a line for three consecutive instants t^{S}.

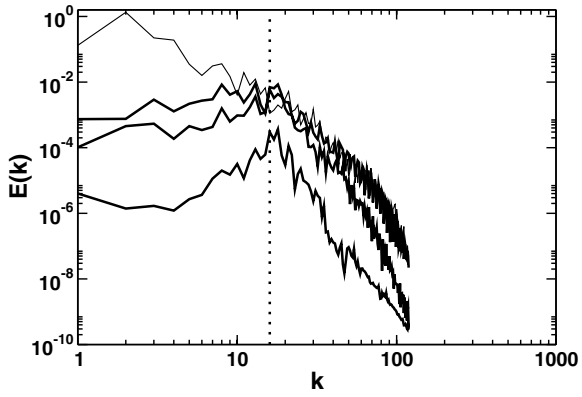

Fig. 9. Time evolution of the SS energy spectra (solid line) compared with the DNS spectrum (thin solid line) on a line for three consecutive instants of t^{S}. The LS grid resolution is shown by dotted vertical line.

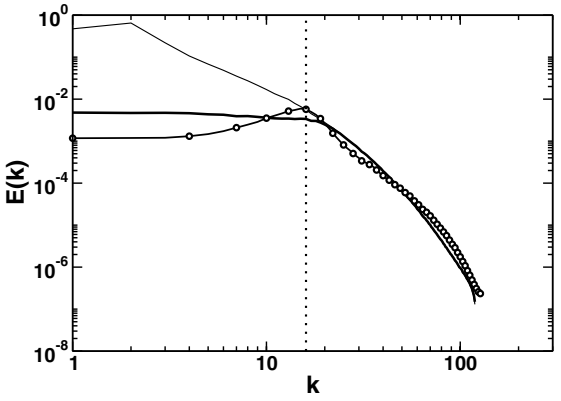

Fig. 10. Average line energy spectra: DNS (thin solid line), filtered SS (solid line), reconstructed SS (circles). LS grid resolution is shown by dotted vertical line.

(i) At the m-th time step t_m^{L}, interpolate u_i^{L} and p^{L} onto each line l_k, such that

$$u_i^{\mathrm{L}}(\mathbf{x}_n, t_m^{\mathrm{L}}) \to u_{i,l_k}^{\mathrm{L}}(l_k, t_m^{\mathrm{L}}), \quad p^{\mathrm{L}}(\mathbf{x}_n, t_m^{\mathrm{L}}) \to p_{l_k}^{\mathrm{L}}(l_k, t_m^{\mathrm{L}}), \qquad \mathbf{x}_n \in l_k$$

(ii) Evolve Eq. (26) on each line l_k with zero initial condition and corresponding boundary conditions until the SS energy is matched with the LS energy at the LS grid minimal resolvable scale to obtain the SS velocity field $u_{i,l_k}^{\mathrm{S}}(l_k, t_m^{\mathrm{L}})$;

(iii) For all LS grid points $\mathbf{x}_n$ calculate the mutual tensor product of the SS velocity $\left[u_i^{\mathrm{S}} u_j^{\mathrm{S}}\right]^{\mathrm{L}}$ as well as the mixed tensor products $\left[u_i^{\mathrm{S}} u_j^{\mathrm{L}}\right]^{\mathrm{L}}$ and $\left[u_i^{\mathrm{L}} u_j^{\mathrm{S}}\right]^{\mathrm{L}}$ by averaging over three lines intersecting at the LS grid point $\mathbf{x}_n$ belonging to the cell V_n, according to Eq. (24):

$$\left[u_i^{\mathrm{S}} u_j^{\mathrm{S}}\right]^{\mathrm{L}}(\mathbf{x}_n, t_m^{\mathrm{L}}) \leftarrow \left[u_{i,l_k}^{\mathrm{S}} u_{j,l_k}^{\mathrm{S}}(l_k, t_m^{\mathrm{L}})\right]_{l_k}, \quad \left[u_i^{\mathrm{S}} u_j^{\mathrm{L}}\right]^{\mathrm{L}}(\mathbf{x}_n, t_m^{\mathrm{L}}) \leftarrow \left[u_{i,l_k}^{\mathrm{S}} u_{j,l_k}^{\mathrm{L}}(l_k, t_m^{\mathrm{L}})\right]_{l_k}$$

(iv) Advance the LS fields $u_i^{\mathrm{L}}(\mathbf{x}_n, t_m^{\mathrm{L}})$, $p^{\mathrm{L}}(\mathbf{x}_n, t_m^{\mathrm{L}})$ to the next time level $t_{m+1}^{\mathrm{L}} = t_m^{\mathrm{L}} + \Delta t^{\mathrm{L}}$ by integrating the LS equations.

5. TLS of forced isotropic turbulence

The forced isotropic turbulence presents the important ideal case to evaluate turbulence modeling approaches. TLS of the forced isotropic turbulent flow has been conducted to study the ability of the model to sustain the stationary turbulent state at the LS and the SS levels, and to provide an adequate energy coupling between LS and SS.

A uniform 32^3 LS grid is used to discretize 2π cubic domain. A standard, second order projection method of van Kan [43] is employed to solve the LS equations. Spatial discretization is done on the staggered grid using finite volume formulation. A third-order, low storage Runge–Kutta scheme is employed for temporal discretization [44]. Two cases for the Taylor scale Reynolds number $Re_\lambda \approx 65$ and 114 are considered. All SS lines have uniform resolution of 128 and 256 grid points for the low and high-Reynolds number cases, respectively. A matching DNS for the low Reynolds number case has been also performed by applying the same forcing on 128^3 grid for comparison purposes. For the chosen LS grid resolution, TLS code requires about one single-processor hour on IBM SP4 to reach the stationary turbulent state, while it takes almost 17 h of CPU time for DNS. Both codes were run in serial mode with the exception of the SS computation for the TLS model, which is done in parallel using 48 processors.

Both simulations start with zero initial conditions and periodic in space. The force is concentrated around small wave numbers and gradually drives the flow to the stationary state. Here, we adopt the forcing scheme of Eswaran and Pope [45]. The random force of the form $\hat{f}_i(\mathbf{k}, t) = (\delta_{ij} - k_i k_j/k^2) w_j(\mathbf{k}, t) \times [\Theta(\mathbf{k}) - \Theta(\mathbf{k} - \mathbf{k}_F)]$ is

used, where w_j is Uhlenbeck–Ornstein stochastic process, δ_{ij} is the Kronecker delta and Θ is the Heaviside function. The process is of diffusion type, has zero mean and correlated over time with a chosen time scale τ. For a given grid resolution, three parameters define the intensity of forcing: the amplitude σ, the time-scale τ and the maximum wave number of the forced modes k_F. Here, we have taken the value of k_F, normalized by the lowest wave number, to be equal to $\sqrt{2}$. With the time scale $\tau = 0.95$ and 0.8, and the amplitude $\sigma = 0.04$ and 0.007, the forcing scheme produces the isotropic turbulent fields with $Re_\lambda \approx 65$ and 114, respectively. However, as it was pointed out by Fureby et al. [46] who used this method to study LES subgrid models, the same forcing cannot be guaranteed for different grid resolutions even with the same forcing parameters. As a result, the DNS case only approximately achieves $Re_\lambda \approx 60$ which is less then $Re_\lambda \approx 65$ of the TLS case. Nevertheless, for comparison purposes it does not appear to be a serious issue.

Time evolution of the root-mean-square (rms) of the LS velocity components $\langle u_i^{\mathrm{L}} \rangle_{\mathrm{rms}}$ along with the averaged rms-velocity scale are shown in Fig. 11(a). It is seen that the stationary state is reached at time $T \approx 8$ for both cases. Fig. 11(b) shows the compensated energy spectra of TLS and DNS cases after the stationary state is reached. Both TLS energy spectra approximate the DNS spectrum quite satisfactorily. These figures suggest that TLS is able to sustain the turbulent stationary state well and the SS coupling does not destroy the isotropy of the LS flow.

However, TLS cases result in a small build-up of energy near the LS cut-off wave number. It can be related to the fact that the SS velocity field might be underestimated on some lines, thus providing diminished dissipative effects on scales at the LS grid cut-off level. In TLS, the SS fields are evolving from zero to the point when the LS and SS spectra are matched at the minimum resolvable LS scales. Generally, the SS evolution time, which is required to match LS and SS spectra, is different for various lines. Matching spectral condition

is important to simulate correct coupling between the LS and the SS velocity fields. If the SS field grows too much it would produce unphysical effects on the LS field by backscattering extra energy at the LS grid level, eventually contaminating the LS field. On the other hand, if the SS field is underpredicted in spectral magnitude at the LS grid cut-off level, it would not provide enough dissipation to the LS field causing the energy pile-up by blocking forward cascade.

The SS evolution time is also a function the local Reynolds number and the LS grid resolution. The more LS are resolved the less time is needed to reconstruct the SS field and vice versa. On the other hand, the higher the Reynolds number, the larger is the range of scales that is needed, and longer time is required to fill up the modeled SS part of the spectrum. Further study is needed to address the SS evolution time sensitivity to the LS grid resolution and the Reynolds number.

6. Conclusion

A novel approach, which is alternative to traditional LES, two level simulation has been developed based on the explicit simulation of the small-scale velocity fields. A coupled system of the large and small-scale governing equations, that is not based on an eddy-viscosity type of assumptions and requires no adjustable parameters, has been derived based on the decomposition of flow fields into the large-scale and the small-scale components. To alleviate complexity of simulation, the small-scale equation has been treated on a domain with a reduced dimension representing a collection of 1D lines. The small-scale equation has been studied by simulating the forced isotropic turbulence. Reconstruction of the SS field in 3D requires some modeling since SS derivatives in the directions transverse to the line direction are not available. To validate SS model assumptions statistical analysis of the SS derivatives has been performed based on DNS data set. It has been shown that the resulting simplified SS velocity equation is able to reconstruct the SS velocity based on the LS velocity field only, without invoking the eddy-viscosity hypothesis or using modeling constants. Fully coupled implementation of TLS has been demonstrated for a case of the forced isotropic turbulence at $Re_\lambda \approx 65$ and 114.

The current approach is readily extendable to treat high-Re non-homogeneous turbulent flows. *A priori* analysis of the SS derivatives for a high-Re turbulent channel DNS data shows strong similarity with the SS derivatives of the homogeneous and isotropic turbulence. This can provide a certain level of justification to use the modeled SS equation for non-homogeneous turbulent flows. This study will be reported in the near future. Overall, results suggest that the TLS approach has the potential for capturing high-Re turbulent flow behavior using rather coarse grids by simulating the SS fields in unresolved flow regions. More importantly, the TLS formulation provides a useful framework for treating complex turbulent flows by not resorting to the concept of the filtering.

Acknowledgments

The authors are grateful to P.K. Yeung for providing isotropic DNS data sets. This work is supported by the Office of Naval Research (Program Manager Dr. Ronald Joslin). Computational time has been provided by DOD HPCC at NAVOCEANO.

References

[1] Y. Kaneda, T. Ishihara, M. Yokokawa, K. Itakura, A. Uno, Energy dissipation rate and energy spectrum in high resolution direct numerical simulation of turbulence in a periodic box, Physics of Fluids 15 (2003) L21–L24.
[2] H. Abe, H. Kawamura, Y. Matsuo, Surface heat-flux fluctuations in a turbulent channel flow up to $Re_\tau = 1020$ with $Pr = 0.025$ and 0.71, International Journal of Heat and Fluid Flow 25 (2004) 404–419.
[3] U. Piomelli, Large-eddy simulation: achievements and challenges, Progress in Aerospace Science 35 (1999) 335–362.
[4] C. Meneveau, J. Katz, Scale-invariance and turbulence models for large-eddy simulation, Annual Review of Fluid Mechanics 32 (2000) 1–32.
[5] C.G. Speziale, Turbulence modeling for time-dependent RANS and VLES – a review, AIAA Journal 36 (1998) 173–184.
[6] S. Ghosal, Mathematical and physical constraints on large eddy simulation of turbulence, AIAA Journal 37 (1999) 425–433.
[7] C. Fureby, G. Tabor, Mathematical and physical constraints on large-eddy simulations, Theoretical and Computational Fluid Dynamics 9 (1997) 85–102.

[8] G.S. Winckelmans, H. Jeanmart, D. Carati, On the comparison of turbulence intensities from large-eddy simulation with those from experiment or direct numerical simulation, Physics of Fluids 14 (2002) 1809–1811.
[9] R.S. Rogallo, P. Moin, Numerical simulation of turbulent flows, Annual Review of Fluid Mechanics 16 (1984) 99–137.
[10] T. Lund, The use of explicit filters in large eddy simulation, Computers & Mathematics with Applications 46 (2003) 603–616.
[11] G. De Stefano, O.V. Vasilyev, "Perfect" modeling framework for dynamic SGS model testing in large eddy simulation, Theoretical and Computational Fluid Dynamics 18 (2004) 27–41.
[12] Y.V. Egorov, M.A. Shubin, Foundations of the classical theory of partial differential equations, Springer, 1998.
[13] O.V. Vasilyev, T.S. Lund, P. Moin, A general class of commutative filters for LES in complex geometries, Journal of Computational Physics 146 (1998) 82–104.
[14] D. Carati, G.S. Winckelmans, H. Jeanmart, On the modelling of the subgrid-scale and filtered-scale stress tensors in large-eddy simulation, Journal of Fluid Mechanics 441 (2001) 119–138.
[15] S. Ghosal, P. Moin, The basic equations for the large eddy simulation of turbulent flows in complex geometry, Journal of Computational Physics 118 (1995) 24–37.
[16] H. van der Ven, A family of large eddy simulation (LES) filters with nonuniform filter width, Physics of Fluids 7 (1995) 1171–1172.
[17] A. Marsden, O. Vasilyev, P. Moin, Construction of commutative filters for LES on unstructured meshes, Journal of Computational Physics 175 (2002) 584–603.
[18] B.J. Geurts, A. Leonard, Is LES ready for complex flows? Closure Strategies for Turbulent and Transitional Flows, Cambridge University Press, 2002.
[19] F. van der Bos, B.J. Geurts, Commutator errors in the filtering approach to large-eddy simulation, Physics of Fluids 17 (2005) 035108–035120.
[20] F. van der Bos, B.J. Geurts, Lagrangian dynamics of commutator errors in large-eddy simulation, Physics of Fluids 17 (2005) 075101–075115.
[21] D.R. Chapman, Computational aerodynamics, development and outlook, AIAA Journal 17 (1979) 1293–1313.
[22] K. Kemenov, S. Menon, A two-level simulation methodology for LES of high Reynolds number flows, in: Advances in Turbulence IX, CIMNE, 2002, pp. 203–206.
[23] K. Kemenov, S. Menon, Two level simulation of high-*Re* turbulent flows, in: Direct and Large-Eddy Simulation V, Proceedings of the Fifth International ERCOFTAC WorkshopErcoftac Series, vol. 9, Kluwer, 2004, pp. 49–56.
[24] E. Hylin, J. McDonough, Chaotic small-scale velocity fields as prospective models for unresolved turbulence in an additive decomposition of the Navier–Stokes equation, International Journal of Fluid Mechanics Research 26 (1999) 539–567.
[25] T. Dubois, F. Jauberteau, R. Temam, Incremental unknowns, multilevel methods and the numerical simulation of turbulence, Computer Methods in Applied Mechanics and Engineering 159 (1998) 123–189.
[26] T. Dubois, F. Jauberteau, A dynamic multilevel model for the simulation of the small structures in homogeneous isotropic turbulence, Journal of Scientific Computing 13 (1998) 323–367.
[27] T. Hughes, L. Mazzei, K. Jansen, The large eddy simulation and variational multiscale method, Computing and Visualization in Science 3 (2000) 47–59.
[28] T. Hughes, L. Mazzei, A. Oberai, The multiscale formulation of large-eddy simulation: decay of homogeneous isotropic turbulence, Physics of Fluids 13 (2001) 505–512.
[29] T. Hughes, A. Oberai, L. Mazzei, Large eddy simulation of turbulent channel flows by variational multiscale method, Physics of Fluids 13 (2001) 1784–1799.
[30] J.-P. Laval, B. Dubrulle, S. Nazarenko, Nonlocality of interaction of scales in the dynamics of 2D incompressible fluids, Physical Review Letters 83 (1999) 4061–4064.
[31] J.-P. Laval, B. Dubrulle, S. Nazarenko, Nonlocality and intermittency in three-dimensional turbulence, Physics of Fluids 13 (2001) 1995–2012.
[32] B. Dubrulle, J.-P. Laval, S. Nazarenko, N.-R. Kevlahan, A dynamic subfilter-scale model for plane parallel flows, Physics of Fluids 13 (2001) 2045–2064.
[33] J.-P. Laval, B. Dubrulle, S. Nazarenko, Fast numerical simulations of 2D turbulence using a dynamic model for subfilter motions, Journal of Computational Physics 196 (2004) 184–207.
[34] C. Foias, O. Manley, R. Temam, Approximate inertial manifolds and effective viscosity in turbulent flows, Physics of Fluids A 3 (1991) 898–911.
[35] O. Manley, R. Temam, W. Shouhong, Inertial manifolds, partially space-averaged equations, and the separation of scales in turbulent flows, Physics of Fluids 7 (1995) 1791–1793.
[36] F. Bouchon, F. Jauberteau, A multilevel method applied in the nonhomogeneous direction of the channel flow problem, Applied Numerical Mathematics 36 (2001) 1–34.
[37] S.S. Collis, Monitoring unresolved scales in multiscale turbulence modeling, Physics of Fluids 13 (2001) 1800–1806.
[38] B. Knaepen, O. Debliquy, D. Carati, Large-eddy simulation without filter, Journal of Computational Physics 205 (2005) 98–107.
[39] P.K. Yeung, Y. Zhou, On the universality of the Kolmogorov constant in numerical simulations of turbulence, Physical Review E 56 (1997) 1746–1752.
[40] J.-L. Guermond, J.T. Oden, S. Prudhomme, Mathematical perspective on large eddy simulation models for turbulent flows, Journal of Mathematical Fluid Mechanics 6 (2004) 195–248.
[41] U. Piomelli, E. Balaras, Wall layer models for large eddy simulation, Annual Review of Fluid Mechanics 34 (2002) 349–374.
[42] C. Beck, Superstatistics in hydrodynamic turbulence, Physica D 193 (2004) 195–207.

[43] J. van Kan, A second-order accurate pressure-correction scheme for viscous incompressible flow, SIAM Journal of on Scientific and Statistical Computing 7 (1986) 870–891.
[44] J.H. Williamson, Low-storage Runge–Kutta schemes, Journal of Computational Physics 35 (1980) 48–56.
[45] V. Eswaran, S.B. Pope, An examination of forcing in direct numerical simulations of turbulence, Computers and Fluids 16 (1988) 257–278.
[46] C. Fureby, G. Tabor, H.G. Weller, A.D. Gosman, A comparative study of subgrid scale models in homogeneous isotropic turbulence, Physics of fluids 9 (1997) 1416–1429.